Modelling Handed Shearing Auxetics: Selective Piecewise Constant Strain Kinematics and Dynamic Simulation

Stölzle, Maximilian; Chin, Lillian; Truby, Ryan; Rus, Daniela; Della Santina, Cosimo

DOI
10.1109/RoboSoft55895.2023.10121989

Publication date
2023

Document Version
Final published version

Published in
Proceedings of the IEEE International Conference on Soft Robotics, RoboSoft 2023

Modelling Handed Shearing Auxetics: Selective Piecewise Constant Strain Kinematics and Dynamic Simulation

Maximilian Stölzle, Lillian Chin, Ryan L. Truby, Daniela Rus, and Cosimo Della Santina

2023 IEEE International Conference on Soft Robotics (RoboSoft) | 979-8-3503-3222-3/23/$31.00 ©2023 IEEE | DOI: 10.1109/ROBOSOFT55895.2023.10121989

***Abstract*— Electrically-actuated continuum soft robots based on Handed Shearing Auxetics (HSAs) promise rapid actuation capabilities while preserving structural compliance. However, the foundational models of these novel actuators required for precise control strategies are missing. This paper proposes two key components extending discrete Cosserat rod model (DCM) to allow for modeling HSAs. First, we propose a mechanism for incorporating the auxetic trajectory into DCM dynamical simulations. We also propose an implementation of this extension as a plugin for the Elastica simulator. Second, we introduce a Selective Piecewise Constant Strain (SPCS) kinematic parameterization that can describe an HSA segment's shape with fewer configuration variables. We verify both theoretical contributions experimentally. The simulator is used to replicate experimental data of the mechanical characterization of HSA rods. For the second component, we attach motion capture markers at various points to a parallel HSA robot and find that the shape of the HSAs can be kinematically represented with an average accuracy of 0.3 mm for positions and 0.07 rad for orientations.**

I. Introduction

Continuum soft robots promise natural compliance and safe interaction with humans, thanks to their invertebrate-inspired bodies [1]. Several actuation technologies for soft robots have been explored in recent years, with the most popular being cable-driven and pneumatic actuation [2].

Handed Shearing Auxetics (HSA) robots are a recent development in this field [3]–[5], which directly transform applied motor torques into complex motion primitives. This novel type of actuator is based on an architected metamaterial. The most important characteristic of this cylindrical metamaterial is that twist strains along the handedness of the structure lead to an elongation of the rod, which is also called auxetic trajectory [6]. An HSA robot combines multiple HSAs of different handedness with a platform constraining the movement of the distal ends in the fashion of a soft parallel manipulator. Differential elongation of the rods enables complex motion primitives such as elongation, bending, and twisting [3], which can be seen in Fig. 2. HSA robots are particularly difficult to model and control as the forces and torques causing the evolution of the system are not directly produced by the actuator, but instead are intrinsically generated as an effect of the modified cell state of the metamaterial and of the interaction forces coming from the parallel arrangement.

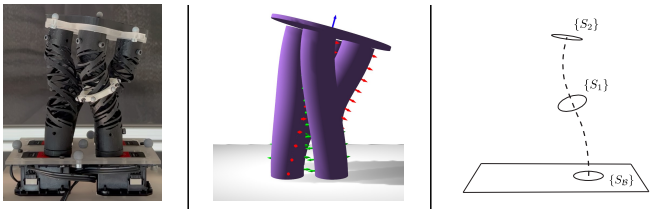

Fig. 1: An HSA robot in a twisted state: simulation and schematic of kinematic model of single HSA rod.

Finite Element Method (FEM) based approaches [7] have proven to be effective in simulating soft parallel structures [8] and could be a good candidate for representing the complex behavior of HSA robots. However, in this paper we strive for a less computationally expensive solution - towards applications in model based control [9]. For this reason, we look at the framework of the Discretized Cosserat Rod Model (DCM). The Cosserat rod theory assumes the slenderness of the object, e.g. that the length is much larger than the radius, and allows for the rod to exhibit all six principal strains. The 1D discretization of the rod along its length dramatically reduces the computational demand compared to FEM [10]. Several works in recent literature have successfully applied this framework to soft robotics [11]–[13]. Among them, in Piecewise Constant Strain (PCS) [14] the continuum dynamics of the Cosserat model is discretized in space by keeping a selection of strains constant along a segment of the continuum. The most popular PCS is Piecewise Constant Curvature (PCC) [15], which assumes a sequence of arcs. Functional extensions of PCS use continuous function to approximate the strain [16], [17].

However, none of these methods are currently applicable to HSA robots, as they do not embed a mechanism for incorporating the effect of the auxetic trajectory. We are aware of just one work looking into kinematic modeling of HSA robots [18], which however models the backbone of the robot with PCC instead of modeling the HSAs. As a consequence, the model cannot represent complex behaviors of the module, like the twist in Fig. 1.

The goal of this paper is to provide such a mechanism, to introduce a strategy for further reducing the dimensionality of the model, and to provide extensive experimental validation to both. More specifically, our extension to the DCM framework couples the twist strain of the HSA rod to its rest length. Additionally, we allow the rigidity of the rod to be modified as a function of the twist strain. We have implemented this mechanism as a plugin for Elastica [19], which we provide open source [1]. This results in a compact dynamic model that

The work by Maximilian Stölzle was in part supported under the European Union's Horizon Europe Program from Project EMERGE - Grant Agreement No. 101070918.

M. Stölzle and C. Della Santina are with the Cognitive Robotics department, Delft University of Technology, Mekelweg 2, 2628 CD Delft, Netherlands. {M.W.Stolzle, C.DellaSantina}@tudelft.nl L. Chin, and D. Rus are with the MIT Computer Science and Artificial Intelligence Laboratory (CSAIL), Massachusetts Institute of Technology, Cambridge, MA 02139 USA, ltchin@mit.edu, rus@csail.mit.edu R. Truby is with the Departments of Materials Science & Engineering and Mechanical Engineering, Northwestern University, Evanston, IL 60208 USA, rtruby@northwestern.edu C. Della Santina is also with the Institute of Robotics and Mechatron- ics, German Aerospace Center (DLR), 82234 Weßling, Germany

[1] https://github.com/tud-cor-sr/HSA-PyElastica

we test experimentally.

We then use a combination of Constant Strain (CS) and PCSs [14] to describe the shape of HSA rods, which we call a Selective Piecewise Constant Strain (SPCS) model: while some strains, such as twist & stretch, are mostly constant over the length of the entire HSA, other strains such as bend & shear significantly vary and are thus captured in a piecewise parametrization. We provide an open-source implementation of this kinematic model in JAX [2].

In summary, we contribute to the state of the art in modeling of soft robots with:

1) A mechanism for integrating the auxetic trajectory of HSAs into the discrete Cosserat rod theory [10], [20].
2) A plugin for the Elastica simulator [19], which also includes the necessary boundary conditions and joint formulations to simulate HSA robots.
3) A Selective Piecewise Constant Strain (SPCS) kinematic model to parameterize the shape of HSAs with a dramatically reduced number of states.

Contributions (1) and (2) are covered in Section II. Subsequently, we introduce the kinematic model from contribution (3) in Section III and verify it in Section IV.

II. Dynamic simulation of HSA robots

We introduce a new concept to enable the simulation of HSA robots with the discretized Cosserat rod theory, which is used by many of the SoA simulators of soft continuum robots [19], [20]. While we provide an implementation of the proposed concept as a plugin to Elastica [19], the same strategy could be used to adapt other simulators such as SoRoSim [20] to HSA robots. We give some background on the DCM in Section II-A. Then, in II-B, we propose a mechanism to infuse the auxetic trajectory for a HSA into the DCM framework. Subsequently, we verify the steady-state behaviour of an HSA against the mechanical characteristics in II-C. Next, we lay out in II-D the necessary boundary conditions of the HSAs and describe the joint mechanism connecting the platform with the rods. Finally, we explain in Section II-E how we were able to reproduce in simulation the main motion primitives of HSA robots.

A. Background: Discretized Cosserat-rod model

This subsection will introduce the governing equations of the DCM following the work by Gazzola et al. [10]. According to the Cosserat rod theory, a slender rod's shape can be purely described by the line along its backbone. The backbone curve is divided into a discrete set of nodes with position $r_i(t) \in \mathbb{R}^3$ for $i \in \{1, \dots, n_\mathrm{v}+1\}$ and n_v links of orientation $Q_i(t) \in \mathbb{R}^{3\times3}$. Differentiating the position and orientation with respect to time gives the translational and angular velocities $v_i = \frac{\partial r_i}{\partial t} \in \mathbb{R}^3$ and $\omega^i_{\mathcal{L}} \in \mathbb{R}^3$. Each node has a mass of m_i and the rigid links are modelled to have a second mass moment of inertia J_i. When a rod of unstretched length $\hat{L}$ is at rest, each link has a length of $\hat{l}_i$ and connects two consecutive vertices. The circumflex accent will denote quantities in the rest configuration of the rod. When the rod is in a deformed state, l describes the current edge length and the shear and axial strains are considered in the vector $\sigma = \begin{pmatrix}\sigma_x & \sigma_y & \sigma_z\end{pmatrix}^\mathrm{T}$. The curvature vector $\kappa_{\mathcal{L}} = \begin{pmatrix}\kappa_x & \kappa_y & \kappa_z\end{pmatrix}^\mathrm{T}$ captures the bending and twist strains. All strains are defined with respect to the rest length of the link $\hat{l}_i$ and the dilation factor $e_i = \frac{l_i}{\hat{l}_i}$ denotes the deviation from that rest length. The shear and stretch stiffness is specified through the diagonal matrix $S = \mathrm{diag}(EI_{xx}, EI_{yy}, GI_{zz}) \in \mathbb{R}^{3\times3}$, where E, G are the elastic and shear modulus respectively, and $I \in \mathbb{R}^{3\times3}$ is the second area moment of inertia. Analogue, the bending and twist rigidity is stored in $B = \mathrm{diag}(B_x, B_y, B_z) \in \mathbb{R}^{3\times3}$. For conciseness, we include below only the equation for the translational accelerations. We refer the interested reader to [10] for the equation on rotational accelerations and more complimentary details about the DCM.

$$m_i \frac{\partial v_i}{\partial t} = \Delta^h \left(\frac{Q_i^\mathrm{T} \hat{S}_i \sigma^i_{\mathcal{L}}}{e_i} \right) + F_i, \quad i \in \{1, \dots, n_\mathrm{v}+1\}, \tag{1}$$

where $F_i \in \mathbb{R}^3$ is the external force acting on the ith vertex. Several quantities are expressed in the Voronoi domain $\mathcal{D}$, in which the length of the region $\mathcal{D}_i$ can be computed as $\mathcal{D}_i = \frac{l_{i+1}+l_i}{2}, i \in [1, n_\mathrm{v}-1]$. Examples are the the Voronoi curvature $\hat{\kappa}^i_{\mathcal{L}}$ over the interior vertices, and the bend twist stiffness matrix $\hat{B}_i$. $\Delta^h : \{\mathbb{R}^3\}_N \to \{\mathbb{R}^3\}_{N+1}$ is used as the discrete difference operator.

B. Auxetic trajectory

We propose several adjustments to the standard definition of the DCM to allow for realistic simulation of HSAs. The main assumption behind the proposed concept is that twist strains agreeing with the handedness of the rod will modify the internal angle between the auxetic pattern cells and with that also change the system characteristics such spring constant, blocked force, etc.

Most importantly, we introduce a distinction between the the printed, initial, length of the HSA $\bar{L}$ and the rest length of the rod $\hat{L}$. This allows us to mirror the auxetic trajectory, as the minimum energy length is increased with applied twist angles / strains [6]. Similar to the HAT accent, which denotes rest quantities, the BAR accent will point out quantities of the HSA in the initial / printed state. We propose to linearly scale the edge rest length $\hat{l}_i$ with the twist strain $\kappa^i_{\mathcal{L},z}$:

$$\hat{l}_i = (1 + \varepsilon_i)\, \bar{l} \quad i \in \{1, \dots, n_\mathrm{v}+1\}, \tag{2}$$

$$\varepsilon_i = \max\left(\min\left(h\, C_\varepsilon\, \mathcal{A}^h(\kappa^i_{\mathcal{L},z}), \varepsilon_{\max}\right), \varepsilon_{\min}\right). \tag{3}$$

In this expression, the twist strain $\kappa^i_{\mathcal{L},z}$ is elevated from the Voronoi to the vertex domain with the averaging operator $\mathcal{A}^h : \{\mathbb{R}^3\}_N \to \{\mathbb{R}^3\}_{N+1}$. $h \in \{-1, 1\}$ is the handedness of the rod. Right is defined as the positive, and left as the negative handedness. C_ε is the extension factor, which needs to be tuned with respect to the chosen auxetic pattern. The minimum and maximum extension $\varepsilon_{\min}$, $\varepsilon_{\max}$ are the limits of the auxetic trajectory and depend on the HSA type: for example closed HSAs can only exhibit positive elongations [6]. After the rest length is adjusted, the axial stiffness of the rod will guide the current edge length l_i towards the (target) edge rest length. Furthermore, we recall the definition of bend / twist strains: $\kappa^i_{\mathcal{L}} = \frac{\log(Q_{i+1}\, Q_i^\mathrm{T})}{\hat{\mathcal{D}}_i}$. To keep the twist strain constant across the entire auxetic trajectory, we define the twist strain with respect to the initial Voronoi length $\bar{\mathcal{D}}_i = \frac{\bar{l}_{i+1}-\bar{l}_i}{2}$:

$$\kappa^i_{\mathcal{L},z} = \frac{\log(Q_{i+1}\, Q_i^\mathrm{T})}{\bar{\mathcal{D}}_i}, \quad i \in \{1, \dots, n_\mathrm{v}+1\} \tag{4}$$

[2] https://github.com/tud-cor-sr/jax-spcs-kinematics

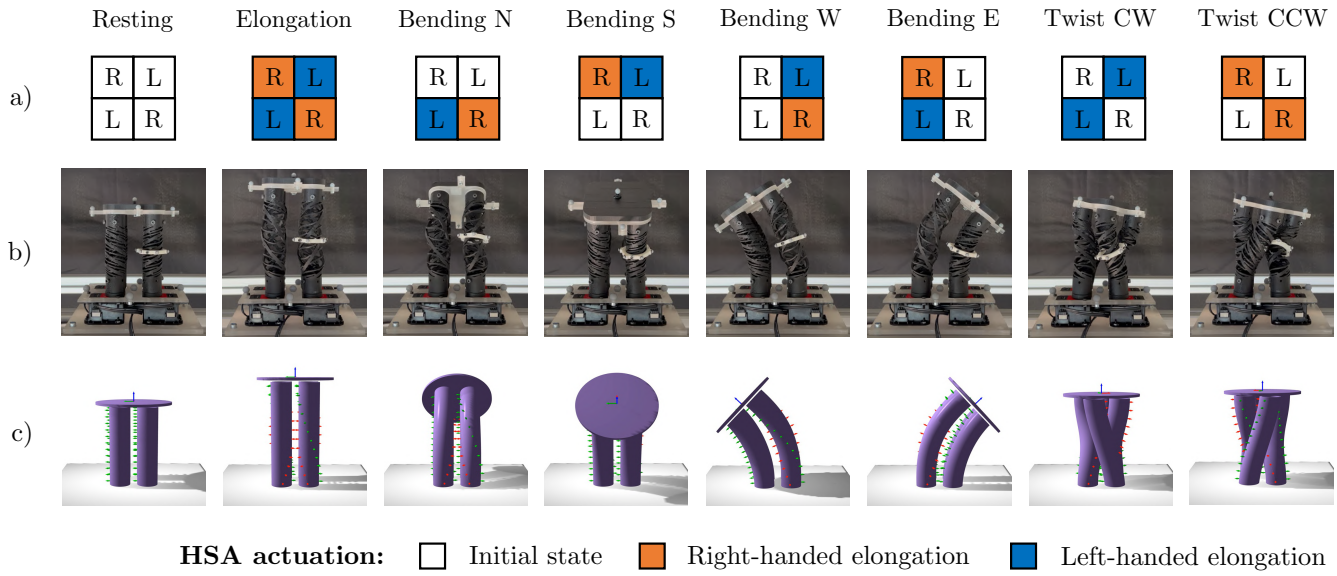

Fig. 2: Motion primitives of Handed Shearing Auxetic (HSA) robots: elongation, bending in the four cardinal directions (e.g. north (N), south (S), west (W), east (E)), and clock-wise (CW) and counter-clockwise (CCW) twisting. **First row (a):** depicts the necessary actuation inputs to generate these motion primitives. Pure elongation is achieved by applying the motor torques of the same magnitude but opposite direction to the left-handed (L) and right-handed (R) HSAs. For bending, there exists a delta in elongation of the rods while the sum of torques is still zero. Last but not least, counter-clockwise twisting is achieved by applying more torque to the right-handed, than to the left-handed HSA rods. **Second row (b):** Snapshots of the experimental platform when actuated according the above specified sequence. **Third row (c):** Renderings of simulated steady-states of an HSA robot. It consists of four HSA rods and a platform at the distal end. The red arrows point along the local x-axis and the green arrows along the local y-axis respectively. The blue arrow signifies the z-axis of the local frame of the platform.

TABLE I: Parameters of simulated HSA rods in Section II-C for various number of HSA row tilings n_{rows}. Row tilings represent the number of vertically stacked unit cells [6]. The rest length $\hat{L}$ and the elastic modulus E are a linear function of the twist strain κ_z. B_z represents the twist rigidity.

n_{rows}	$\hat{L}$ [mm]	E [kPa]	B_z [Nm^2/rad]
4	$75\,(1+3.04\,\kappa_z)$	$576.9+36.1\,\kappa_z$	0.00375
6	$89\,(1+3.50\,\kappa_z)$	$309.3+13.1\,\kappa_z$	0.00213
8	$100\,(1+3.77\,\kappa_z)$	$203.5+10.6\,\kappa_z$	0.00183
10	$112\,(1+3.64\,\kappa_z)$	$197.6+7.5\,\kappa_z$	0.00167
12	$124\,(1+3.53\,\kappa_z)$	$197.6+2.4\,\kappa_z$	0.00124

Finally, recent work by Good et al. [6] has shown that HSAs exhibit special mechanical characteristics, such as that the spring constant increases with the twist angle. Therefore, we allow the shear / stretch and bend / twist rigidity matrices S and B to be modified dynamically during the simulation with the twist strain. For example, for the the axial stiffness of a closed HSA can be modelled as a linear function of the twist strain [6]

$$\hat{S}_z^i = \bar{S}_z^i + C_{S_z}\mathcal{A}^h(\kappa^i_{\mathcal{L},z}), \tag{5}$$

where C_{S_z} is a tunable constant.

C. Verification of single HSA steady-state behaviour

We verify that our simulator can represent the steady-state behaviour of a real HSA by re-producing the characterisation results for closed HSAs by Good et al. [6]. More specifically, we let the simulator converge to steady-state and then identify several mechanical properties such as blocked force (F_{b}), minimum energy length, holding torque (τ_{h}) and the spring constant (k). Following the reporting in [6], we tune the parameters of our simulation to match the behaviour of closed Carbon FPU50 HSAs with 19 mm outside diameter, 2 mm wall thickness, as good as possible. We report the chosen simulation parameters in Table I. The HSA rod is modelled to consist of $n_{\text{v}} = 10$ nodes and 9 links with a material density of $\rho = 1050\,\text{kg/m}^3$. For all simulations, the proximal end of the rod is constrained and only rotations around the z-axis are allowed to mirror the actuation with electric motors. Furthermore, twisting is constrained at the distal end which allows twist strains to build-up in the rod. Otherwise, the distal end is unconstrained.

Next, we will go into more detail about each mechanical characteristic. **Holding torque:** We apply a given torsional torque τ_{h} at the proximal end of the HSA and then record the twist angle of the base ϕ_0 at steady-state. **Minimum energy length:** The proximal end of the HSA is rotated to a given twist angle ϕ_0. The minimum energy length is then is identified as the steady-state length of the HSA. **Spring constant:** For a given twist angle ϕ_0 with the HSA at rest, the spring constant is identified by applying a small pulling force to the distal end and then measuring the displacement of the tip at steady-state. **Blocked force:** Differently from the other simulations, the distal end is constrained at its initial position such as to prevent the rod from extending. The blocked force F_{b} is identified by evaluating the internal axial force for a given twist angle.

The results show that the proposed simulator can accurately represent the steady-state behaviour of the HSAs with the simulated characteristics mostly staying within the stated error-range of the experimental measurements by Good et al. [6]. The only exception is Fig. 3(a), in which the simulation is overestimating the blocked force F_{b}. This points to the fact that this linear approximation of the auxetic trajectory is only accurate in a limited range of the motion range of the

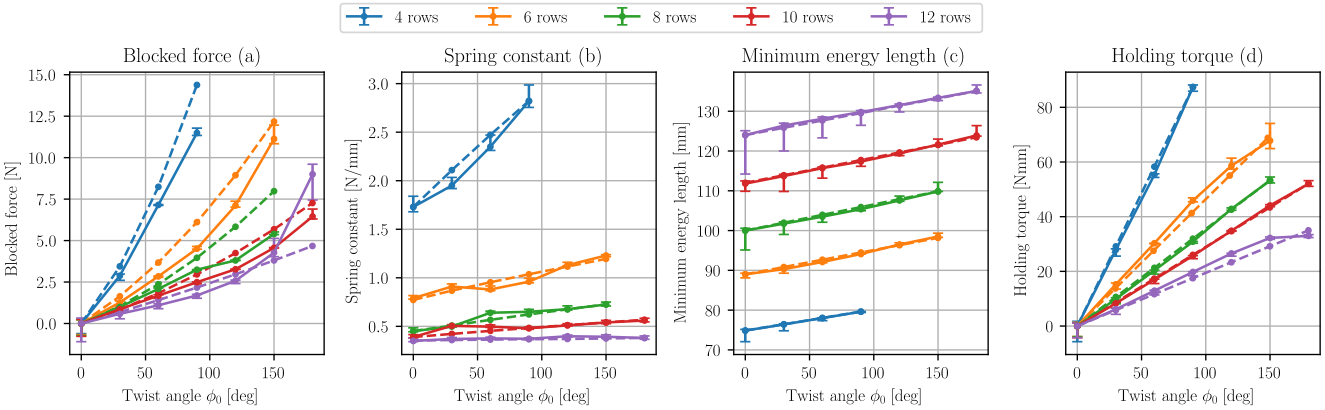

Fig. 3: Results for verification of steady-state behaviour of the proposed simulator: the solid lines represent the mechanical characteristics obtained for closed HSA rods by Good et al. [6] with corresponding error bars. The dashed lines correspond to the same characteristics obtained with our simulator. The simulation parameters are separately tuned for HSAs with variety of row tilings. When an HSA contains a higher number of row tiling, it will allow for larger elongations while simultaneously trading-off the spring constant [6].

closed HSAs. Further research is necessary to come up with auxetic trajectory models for semi-closed and open HSAs.

D. Simulating HSA robots: boundary conditions and joints

We discuss here how to combine a platform and multiple HSAs to form a HSA robot. Assume to have n_{HSA} rods equilly distributed along a circle of radius R_{cHSA} in the x-y plane with the rods pointing towards the positive z-direction in a straight configuration. We need boundary conditions for the proximal ends of the rods to generate the parallel structure. The positions of the proximal nodes are constrained to remain at their initial position $\bar{r}_0$. For the same purpose, the translational rates, e.g. v_0, are set to zero at each time-step.

In our plug-in to Elastica, we provide the user with two options for actuating the HSAs. (a) The orientation of the proximal link Q_0 is moved to a desired orientation Q_0^{d}. In this case, the twist angle ϕ_0^{d} of the proximal end is controlled. Again, the rotational rates ω_0 are set to zero. (b) Twist torques $\tau_{0,z}$ are applied to the proximal link of the HSA. The two remaining rotational DoF (rolling and pitching) of the proximal link are constrained by setting their rotational rates $\omega_{0,x}$ and $\omega_{0,y}$ to zero.

Additionally, rigid joints between the rods and the platform are necessary. These are achieved by simulating a spring-damper system between the distal end of each HSA and the platform. For the translations, we compute the contact force F_{c} as

$$F_{\text{c}} = k_F\,(r_{\text{p}}^j - r_{n_{\text{v}}+1}) + \nu_F\,(v_{\text{p}}^j - v_{n_{\text{v}}+1}), \tag{6}$$

where k_F is the translational joint stiffness, and ν_F the translational damping coefficient. While $r_{n_{\text{v}}+1}$, and $v_{n_{\text{v}}+1}$ are the position and the velocity of the distal node of the rod respectively, r_{p}^j and $v_{n_{\text{v}}+1}^j$) are the position and velocity of the attachment point of the same rod (e.g. the jth rod) on the platform. We determine the position and velocity of this attachment point using rigid body kinematics with regard to the Center of Mass (CoM) of the platform. The contact force F_{c} is applied with an opposite sign to the distal end of the HSA and to the platform, respectively. Please note that the contact force F also generates a torque $\tau_{F_{\text{c}}}$ on the platform, as the force is not applied at the CoM of the rigid body.

Similarly to the contact force, a contact torque τ_{c} is computed to reduce any error in the orientation and angular velocity between the two systems

$$\tau_{\text{c}} = k_\tau\,(Q_{\text{p}}^{\text{T}} \log(Q_{\text{p}}\,Q_{n_{\text{v}}}^{\text{T}})) + \nu_\tau\,(Q_{\text{p}}^{\text{T}}\omega_{\text{p}}^j - Q_{n_{\text{v}}}^{\text{T}}\omega_{n_{\text{v}}}) \tag{7}$$

where the $\log(\cdot) : \mathbb{R}^{3\times3} \rightarrow$ operator computes the rotation vector from the rotation matrix [10], and Q_{p} is the material frame of the platform.

E. Qualitative evaluation of motion primitives in simulation

We reproduce the typical motion primitives of a HSA robot consisting of four HSAs (e.g. $n_{\text{HSA}} = 4$) in simulation and show the final steady-states in Fig. 2. Two of the HSAs are left-handed and positioned diagonally from each other. Each rod is discretized by $n_{\text{v}} = 25$ links and 26 point mass vertices. Furthermore, it has a printed length of $\bar{L} = 100\,\text{mm}$, an outside radius of $25.4\,\text{mm}$ and a wall-thickness of $2.43\,\text{mm}$. The rods are placed at a radial distance of $R_{\text{cHSA}} = 24\,\text{mm}$ from the center of the robot and a material density of $\rho_{\text{HSA}} = 1050\,\text{kg/m}^3$ is assumed. Therefore, the chosen simulation parameters mirror the geometric characteristics of our experimental platform. Based on an elastic modulus $E = 10\,\text{MPa}$ and a shear modulus $G = 0.6\,\text{MPa}$, the shear and stretch stiffnesses amount to $S_{x,y} = 101.5\,\text{N/m}$, and $S_z = 1753.5\,\text{N/m}$. We set the bend and twist rigidities B_x, B_y, and B_z to $0.02\,\text{Nm}^2/\text{rad}$ and $0.014\,\text{Nm}^2/\text{rad}$ respectively. When twist strains are present, we extend the rest length of the rod by $0.01\,\text{m/rad}$ after taking into account the handedness of the HSA.

The cylindrical platform is of diameter $95\,\text{mm}$, has a thickness of $3\,\text{mm}$ and is modelled to have a density of $\rho_{\text{p}} = 700\,\text{kg/m}^3$. The joint stiffness parameters $k_F = 5 \cdot 10^5\,\text{N/m}$ and $k_\tau = 20\,\text{Nm/rad}$ are chosen for the fixed joint between HSAs and platform. The joint damping coefficients ν_F, ν_τ are set to zero.

Our qualitative results in Fig. 2 demonstrate that we are able to generate all motion primitives in simulation. For the shown deformations, we apply maximum twist angles of $\phi_{0,\max} = \pi\,\text{rad}$.

III. A Selective Piecewise Constant Strain Kinematic Model for HSAs

In this section, we aim to derive a forward kinematic model which can be used to describe the shape of an HSA with a

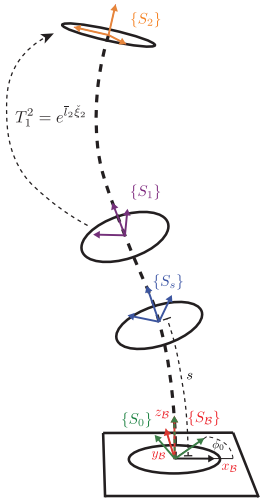

4: Visualization of the proposed SPCS kinematic model for the case of $n_\mathrm{S} = 2$ segments: The forward kinematics describe a transformation from the base frame $\{S_\mathcal{B}\}$ to the local frame $\{S_s\}$ at the coordinate $s \in [0, \bar{L}]$ and consist of a) a rotation around the $z_\mathcal{B}$-axis of the base frame by angle ϕ_0, b) an exponential map $e^{(s-\bar{L}_i)\,\hat{\xi}_i}$ for the transformation from the proximal end of the ith segment to the local frame of the coordinate s.

minimum amount of parameters. More specifically, we want to describe the transformation from the base frame $\{S_\mathcal{B}\}$ to a local frame $\{S_s\}(q, s)$ at a coordinate $s \in [0, \bar{L}]$. This coordinate lies on the backbone of an HSA rod of printed (i.e. initial) length $\bar{L}$. For this purpose, we combine the existing kinematic models CS and PCS [14] to selectively keep specific strains constant along the entire length of the robot or vary them piece-wise among the segments. This parametrization can be combined with the results in Sec. II to generate a compact dynamic model.

First, we define that

$$\xi(q, s) = \begin{pmatrix} \kappa_x & \kappa_y & \kappa_z & \sigma_x & \sigma_y & \sigma_z \end{pmatrix}^\mathrm{T} \in \mathbb{R}^6 \tag{8}$$

represents the three rotational and three linear strains present in a rod [14]. Subsequently, propose the following configuration vector for an HSA

$$q = \begin{pmatrix} \phi_0 & q_\mathrm{CS}^\mathrm{T} & q_{\mathrm{PCS},1}^\mathrm{T} & \cdots & q_{\mathrm{PCS},i}^\mathrm{T} & \cdots & q_{\mathrm{PCS},n_\mathrm{S}}^\mathrm{T} \end{pmatrix}^\mathrm{T} \tag{9}$$

where $\phi_0 \in \mathbb{R}$ is the twist angle at the base and allows for the rotation of the motor actuating the HSA rod. $q_\mathrm{CS} \in \mathbb{R}^{n_{q,\mathrm{CS}}}$ is a strain component constant along the entire rod, and $q_{\mathrm{PCS},i} \in \mathbb{R}^{n_{q,\mathrm{PCS}}}, i \in \{1, \ldots, n_\mathrm{PCS}\}$ is the configuration of each PCS segment. The ith segment has a initial length of $\bar{l}_i$ with its tip at the coordinate $\bar{L}_i$ The strain in the ith segment is then the sum of the rest strain $\hat{\xi} = \begin{pmatrix} 0 & 0 & 0 & 0 & 0 & 1 \end{pmatrix}^\mathrm{T}$, ξ_CS, and $\xi_{\mathrm{PCS},i}$:

$$\xi_i = \hat{\xi} + B_\mathrm{CS}\, q_\mathrm{CS} + B_{\mathrm{PCS},i}\, q_{\mathrm{PCS},i}, \quad i \in \{1, \ldots, n_\mathrm{S}\}. \tag{10}$$

Analogue to the concept introduced in [17], $B_\mathrm{CS} \in \mathbb{R}^{6 \times n_{q,\mathrm{CS}}}$, $B_\mathrm{PCS} \in \mathbb{R}^{6 \times n_{q,\mathrm{PCS}}}$ are the strain bases of q_CS and q_PCS respectively.

In this paper, we specifically investigate a setting where the twist & stretch strains are constant across the entire rod and the bend & shear strains vary for each segment. Accordingly, we choose $q_\mathrm{CS} = \begin{pmatrix} \kappa_z & \sigma_z \end{pmatrix}^\mathrm{T}$ and $q_{\mathrm{PCS},i} = \begin{pmatrix} \kappa_{x,i} & \kappa_{y,i} & \sigma_{x,i} & \sigma_{y,i} \end{pmatrix}^\mathrm{T}$. Then, the corresponding strain bases are determined to be

$$B_\mathrm{CS} = \begin{bmatrix} 0 & 0 & 1 & 0 & 0 & 0 \\ 0 & 0 & 0 & 0 & 0 & 1 \end{bmatrix}^\mathrm{T} \in \mathbb{R}^{6\times 2},$$
$$B_{\mathrm{PCS},i} = \begin{bmatrix} 1 & 0 & 0 & 0 & 0 & 0 \\ 0 & 1 & 0 & 0 & 0 & 0 \\ 0 & 0 & 0 & 1 & 0 & 0 \\ 0 & 0 & 0 & 0 & 1 & 0 \end{bmatrix}^\mathrm{T} \in \mathbb{R}^{6\times 4}. \tag{11}$$

Next, we find homogeneous forward kinematic mappings for the given configuration and strains. As the twist angle ϕ_0 demands a rotation around the local $z_\mathcal{B}$-axis of the base frame,

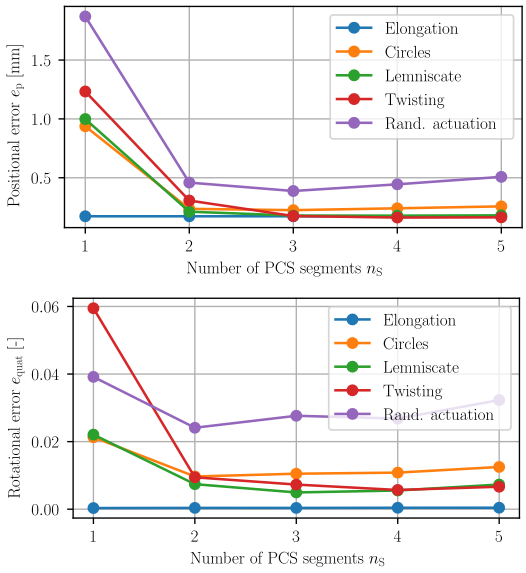

Fig. 5: Verification of kinematic models in simulation. The plot in the first row shows the positional error e_p of the kinematic model against the simulated HSA. The plot in the second row visualizes the rotational error metric e_quat, which is based on the vector component of the unit quaternion. For more information on the evaluation metrics, we refer to Section IV-C. The kinematic model used here assumes the twist & stretch strains to be constant along the entire HSA and the bend & shear strains to be captured by n_S segments. Along this line, we report the performance of the kinematic model for a parametrization containing between one and five segments.

the matrix $R_\mathcal{B}^0(\phi_0) \in SO(3)$ contains the rotation from the base frame $\{S_\mathcal{B}\}$ to the proximal end of the rod denoted as frame $\{S_0\}$. For a point s on the ith segment with constant strain ξ_i, the transformation matrix from the segment's proximal frame $\{S_{i-1}\}$ to the local frame at coordinate s is given by the exponential map $e : \mathfrak{se}(3) \mapsto SE(3)$ [14]

$$\begin{aligned} e^{(s-\bar{L}_{i-1})\hat{\xi}_i} =& I_4 + (s - \bar{L}_{i-1})\,\hat{\xi}_i + \left(1 - \cos((s - \bar{L}_{i-1})\,\theta_i)\right) \\ & \frac{\hat{\xi}_i^2}{\theta_i^2} + \left((s - \bar{L}_{i-1})\,\theta_i - \sin((s - \bar{L}_{i-1})\theta_i)\right) \frac{\hat{\xi}_i^3}{\theta_i^3}. \end{aligned} \tag{12}$$

where $\hat{\xi}_i \in \mathfrak{se}(3)$ is the strain twist vector and $\theta_i = \sqrt{\kappa_{x,i}^2 + \kappa_{y,i}^2 + \kappa_{z,i}^2}$ is the magnitude of the rotational strain. Therefore, the fully assembled transformation $T_\mathcal{B}^i(q)$ from the base frame $\{S_\mathcal{B}\}$ to the tip frame of the ith segment can be expressed as

$$T_\mathcal{B}^i(q) = T_\mathcal{B}^0(\phi_0)\, \Pi_{j=1}^i\, e^{\bar{l}_j \hat{\xi}_j}(q) \in SE(3). \tag{13}$$

IV. Verification of the SPCS Model

The section is structured as follows. We introduce relevant actuation sequences for the HSA robot in IV-A. Next, we present an inverse kinematic approach to identify the kinematic configuration in IV-B. Translational and rotational error metrics are then defined in IV-C to evaluate the quality of reconstructions. Finally, we verify the performance of the proposed SPCS kinematic model both for simulated data (IV-D) and on experimental datasets (IV-E). The code and all datasets are made available on GitHub [3].

[3] https://github.com/tud-cor-sr/hsa-kinematic-model

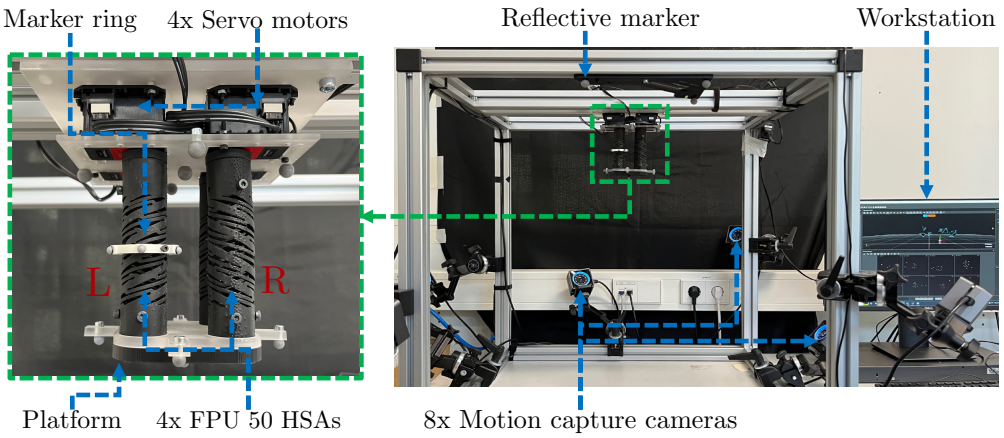

6: Experimental setup with the HSA robot attached in platform-down configuration to the motion capture cage. The robot contains two left-handed (L) and two right-handed (R) HSA rods respectively. Rods of the same handedness are placed opposite of each other. The reflective markers allow us to determine the pose information of the base, an intermediate point along the left HSA rod, and the platform.

A. Actuation sequences

We collect datasets with a variety of actuation sequences, which includes both pure motion primitives and random actuation. For all sequences, we apply a twist angle of magnitude $|u_\mathrm{d}| \in [0, \pi \text{ rad}]$ at the base of each HSA. The sign of u_d is determined by the handedness h of the respective HSA. The elongation dataset consists of samples between the rest and fully-elongated HSA state. Please refer to Fig. 2(a) for more details how each motion primitive can be invoked. For the bending motion primitive, we consider two separate trajectory types: a) a Lemniscate trajectory and b) a trajectory containing circles of varying bending angles. The different bending angles are achieved by varying the actuation angle from 20 % to 100 % of its maximum magnitude. For each fixed bending angle, we collect 15 samples along the circle, e.g. 15 different azimuth angles. To achieve the desired azimuth angle, we smoothly interpolate between the east, north, west, and south actuation specifications of Fig. 2(a). The twisting trajectory collects discrete samples between maximum clockwise (CW) and maximum counter-clockwise (CCW) twisting. Finally, we collect a dataset of randomly sampled actuation inputs, which combines the elongation, bending, and twisting motion primitives. In total, the elongation and Lemniscate trajectories contain 100 samples each, the circles and twisting trajectory have 225 and 100 samples respectively. 500 samples are included in the random actuation actuation sequence.

B. Inverse Kinematics

Differential inverse kinematics can be used to reconstruct the rod's configuration q from N known poses $T_\mathcal{B}^{s_i} \in SE(3), i \in [1, N]$ along the rod. We implemented an inverse kinematics algorithm based on the analytical Jacobian $J_\mathrm{A}^{s_i} \in \mathbb{R}^{6\times7}$ of the pose representation

$$\chi_\mathcal{B}^{s_i} = \begin{pmatrix}\varepsilon_x & \varepsilon_y & \varepsilon_z & \eta & \varepsilon_z & p_x & p_y & p_z\end{pmatrix}^\mathrm{T} \in \mathbb{R}^7,$$

which includes rotational orientation estimates in unit quaternion representation $\mathcal{Q} = \begin{pmatrix}\varepsilon_x & \varepsilon_y & \varepsilon_z & \eta\end{pmatrix}^\mathrm{T}$ and positions in Cartesian space $p = \begin{pmatrix}p_x & p_y & p_z\end{pmatrix}^\mathrm{T}$. Please note that usually ϕ_0 does not need to be found through (differential) inverse kinematics, but can rather be directly be read-out from the encoders of the electric servos. All N poses and Jacobians can be vertically stacked as $\chi \in \mathbb{R}^{7N}$ and $J_\mathrm{A} \in \mathbb{R}^{7N\times6}$ respectively. This then allows us to then iteratively optimize the pose error $e_\chi = \chi_\mathrm{d} - \tilde{\chi}$ between the known pose χ_d and the pose $\tilde{\chi}$ computed using the forward kinematics

$$\tilde{q}_{\mathrm{it}+1} = \tilde{q}_\mathrm{it} + \lambda\, J_\mathrm{A}^\mathrm{T}(\tilde{q})\,\left(\chi_\mathrm{d} - \tilde{\chi}(\tilde{q})\right), \tag{14}$$

where $\tilde{q}$ is the current configuration estimate, and λ is the step size.

C. Evaluation metrics

We briefly introduce the metrics to quantify shape reconstruction accuracy by the proposed kinematic parametrization. We first define a Root Mean-Squared Error (RMSE) for comparing each ground-truth position $p_t^i \in \mathbb{R}^3, t \in \{1, \ldots, n_t\}, i \in \{1, \ldots, N\}$ to the position estimated by the kinematic model $\tilde{p}_t^i$ over a time period of n_t steps

$$e_\mathrm{p} = \sqrt{\sum_{t=1}^{n_\mathrm{t}}\sum_{i=1}^{N} \frac{\left(\left\|\tilde{p}_t^i - p_t^i\right\|_2\right)^2}{n_\mathrm{t}\, N}} \in \mathbb{R}. \tag{15}$$

The rotational RMSEs e_quat is computed analogue by substituting p in (15) with the quaternion vector component $\varepsilon = \begin{pmatrix}\varepsilon_x & \varepsilon_y & \varepsilon_z\end{pmatrix}^\mathrm{T}$. Finally, we compute the XYZ Euler angle error as

$$e_\mathrm{eul} = \sqrt{\sum_{t=1}^{n_\mathrm{t}}\sum_{i=1}^{N} \frac{\left(f_\vartheta(R_{t,i}\,\tilde{R}_{t,i}^\mathrm{T})\right)^2}{n_\mathrm{t}\, N}} \in \mathbb{R}^3, \tag{16}$$

where $f_\vartheta(\cdot)$ is the operator to compute the XYZ Euler angles $\vartheta = \begin{pmatrix}\alpha & \beta & \gamma\end{pmatrix}^\mathrm{T}$ from a rotation matrix $R \in SO(3)$.

D. Simulation results

We employ the higher dimensional HSA robot simulator proposed in Section II to generate steady-state HSA states. We use the same simulation parameters as in Section II-E. This provides us with 25 discrete poses along each of the four HSAs. Then, we perform differential inverse kinematics with a step size of $\lambda = 0.2$ to find an optimal configuration q describing the shape of the HSA. We choose a higher step size ($\lambda = 1$) for regressing the twist strains.

For the kinematic model, we assume that the twist & stretch strains are constant along the entire HSA rod. The bend & shear strains on the other hand are instead piece-wise constant across n_S segments. We evaluate the influence of the n_S parameter and test the performance of a kinematic model involving between 1 and 5 PCS segments.

The results are in Fig. 5. While a kinematic model with a single CS segment still works sufficiently well for the elongation and bending motion primitives, its performance deteriorates for any trajectories involving twisting. Instead,

TABLE II: Experimental verification of kinematic models on an HSA robot. Motion capture markers attached to one of the HSAs provide with two ground-truth poses along the rod, and we measure ϕ_0 from the servo readings (13 constrains in total). In the spirit of an ablation study, we investigate different variations of the proposed kinematic parametrization. For Constant Curvature (CC), Constant Twist (CT), Constant Shear (CSH), and Constant Axial (CA) strain, the strain is kept constant along the entire HSA. For Piecewise Constant Curvature (PCC), Piecewise Constant Twist (PCT), Piecewise Constant Shear (PCSH), and Piecewise Constant Axial (PCA) strain, the strain components are parameterized separately for each of the two segments. Additionally, we test the importance of including the shear strain component. For each kinematic parametrization, we state the Degrees of Freedom (DoF). We report RMSEs for both translations and rotations (see Sec. IV-C).

Trajectory	**CC**	**CT**	**CSH**	**CA**	**PCC**	**PCT**	**PCSH**	**PCA**	**DoF**	e_{p} [mm]	e_{quat} [-]	$e_{\mathrm{eul},\alpha}$ [rad]	$e_{\mathrm{eul},\beta}$ [rad]	$e_{\mathrm{eul},\gamma}$ [rad]
Elongation	✗	✓	✗	✓	✓	✗	✗	✗	7	1.010	0.0092	0.0029	0.0079	0.0166
Elongation	✗	✓	✗	✓	✓	✗	✓	✗	11	0.126	0.0082	0.0020	0.0031	0.0166
Elongation	✗	✗	✗	✗	✓	✓	✓	✓	13	0.009	0.0042	0.0020	0.0031	0.0070
Circles	✗	✓	✗	✓	✓	✗	✗	✗	7	1.744	0.0136	0.0108	0.0123	0.0228
Circles	✗	✓	✗	✓	✓	✗	✓	✗	11	0.227	0.0082	0.0110	0.0122	0.0227
Circles	✗	✗	✗	✗	✓	✓	✓	✓	13	0.092	0.0093	0.0116	0.0125	0.0075
Lemniscate	✗	✓	✗	✓	✓	✗	✗	✗	7	1.227	0.0098	0.0042	0.0051	0.0195
Lemniscate	✗	✓	✗	✓	✓	✗	✓	✗	11	0.215	0.0082	0.0045	0.0053	0.0195
Lemniscate	✗	✗	✗	✗	✓	✓	✓	✓	13	0.023	0.0052	0.0043	0.0054	0.0076
Twisting	✗	✓	✗	✓	✓	✗	✗	✗	7	2.931	0.0136	0.0121	0.0186	0.0195
Twisting	✗	✓	✗	✓	✓	✗	✓	✗	11	0.263	0.0141	0.0130	0.0196	0.0194
Twisting	✗	✗	✗	✗	✓	✓	✓	✓	13	0.030	0.0127	0.0131	0.0217	0.0017
Rand. actuation	✗	✓	✗	✓	✓	✗	✗	✗	7	4.345	0.0381	0.0678	0.0544	0.0195
Rand. actuation	✗	✓	✗	✓	✓	✗	✓	✗	11	0.365	0.0383	0.0681	0.0544	0.0193
Rand. actuation	✗	✗	✗	✗	✓	✓	✓	✓	13	0.255	0.0380	0.0700	0.0527	0.0200

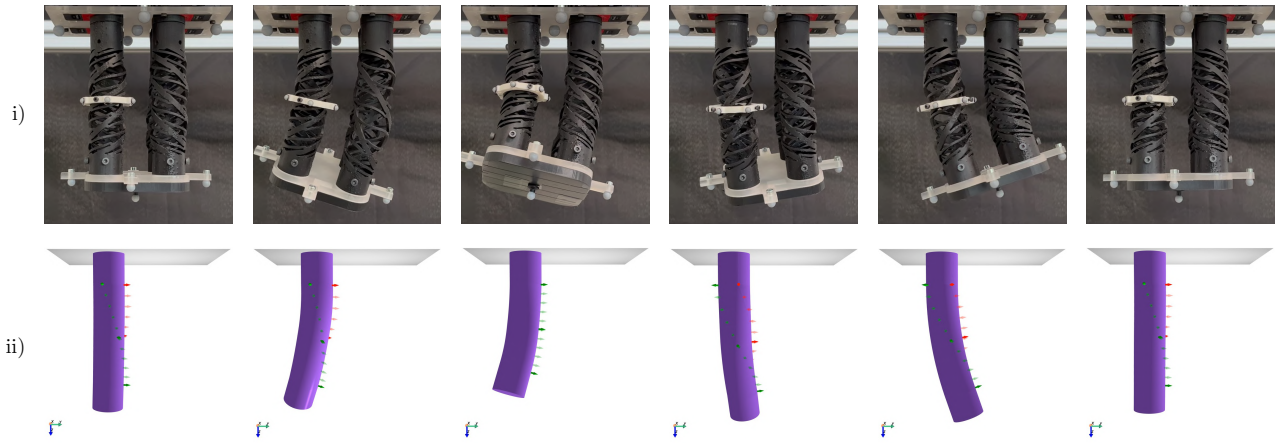

(a) Lemniscate trajectory

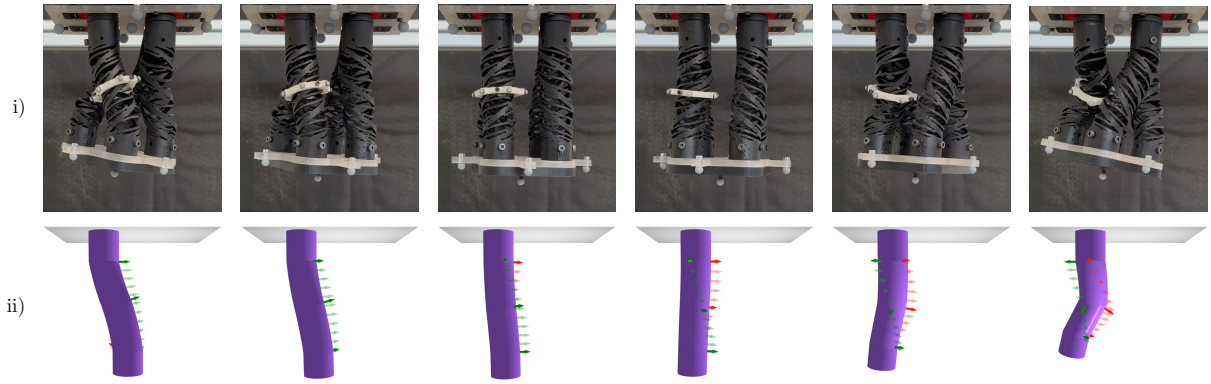

(b) Twisting trajectory

Fig. 7: Sequence of stills for a Lemniscate and a twisting trajectory. **Top row i):** frames of a video recording the HSA robot during the experiments. The shape of the front-left HSA rod is fitted using inverse kinematics and rendered in ii). **Bottom row ii):** Rendered shape of the HSA rod produced by evaluating the forward kinematics along the backbone length. The arrows with full opacity denote the ground-truth pose of three points along the HSA rod as measured by the motion capture system. The red arrow points along the local x-axis and the green arrow along the local y-axis respectively. The arrows with slight transparency represent poses along the backbone computed with the forward kinematics. We assume the last 25 mm and 20 mm at the proximal and distal end of the rod respectively to be rigid and therefore do not include them in the kinematic parametrization.

two segments of our model are sufficient to accurately represent the shape of the HSA.

E. Experimental results

In addition to the simulations, we also experimentally verify the kinematic model using an HSA robot consisting of four closed rods 3D-printed via digital projection lithography from the flexible photopolymer resin Carbon FPU 50 [4]. Each HSA rod was printed to a length of $\bar{L} = 101.6\,\mathrm{mm}$ and is independently actuated by DYNAMIXEL MX-28T servo motors. As seen in Fig. 6, we attach motion capture markers to several points on the robot to track the ground-truth pose information. Namely, we measure the pose of the motor base, the platform, and the midpoint of one of the right-handed HSA rods (i.e. the front-left HSA on the picture). Please note, that we extract the rotation angle ϕ_0 from the servo encoders directly. The robot is mounted at its base to a cubical cage of side length $750\,\mathrm{mm}$ in platform-down configuration. Eight Optitrack Prime X 13 cameras are attached to the cage tracking the reflective markers at $30\,\mathrm{Hz}$.

We actuate the robot from a workstation next-by with the control loop running at $10\,\mathrm{Hz}$. The control loop communicates motor position setpoints $u_\mathrm{d} \in \mathbb{R}^4$ to the servos. The inner control loop of the servos then applies the appropriate torques to guide the motors towards the desired position. As soon as the motors have reached their goal position, we wait for $2\,\mathrm{s}$ to reach steady-state and then read-out the pose measurements.

In Fig. 7, we show sequences of stills for the Lemniscate and twisting trajectory. The kinematic model used here assumes a constant twist strain along the entire rod and employs two PCS segments to capture the remaining five strains. We see that except for extreme twisting states, e.g. the far right image in Fig. 7(b), the kinematic model is able to represent the complex HSA shape very well.

In Tab. II, we quantitatively evaluate multiple kinematic models on the trajectories defined in IV-A. The first (7 DoF) and second (11 DoF) kinematic models are very similar as both assume constant twist and constant stretch along the entire HSA. The other strains are contained in two PCS segments in both cases. However, the first model exhibits much larger positional errors as it neglects shear strains, which are very important in HSA robots, but were not accounted for in the literature [18]. The third model provides the upper bound on the performance, as it has with 12 comparatively many DoF and uses a piecewise formulation with two segments for all segments.

V. Conclusion

This work provided for the first time solutions for modeling the kinematics and the dynamics of electrically-actuated continuum soft robots based on Handed Shearing Auxetics. We have shown that coupling the twist strains to rest lengths can allow simulators based on the discrete Cosserat rod theory. While the proposed linear approximation of the auxetic trajectory works well for closed HSAs within a bounded motion range, future work shall derive a more general model also applicable for semi-closed and open HSAs [6]. Furthermore, we have proposed the SPCS kinematic model that can express the shape of HSAs with 11 DoF. Fitting this kinematic model to the experimental results showed a very good match for representing the shape of the HSAs. In particular for large actuation magnitudes within the twisting motion primitive, the HSAs leave the auxetic trajectory and seem to experience buckling behaviour. For this case, the SPCS model is not accurate anymore. Future work will focus on utilizing the kinematic model proposed in this work for model-based control of HSA robots.

Acknowledgment

We thank I. Good and J. Lipton from the University of Washington, U.S. for sharing the mechanical characterisation published in [6]. We also acknowledge S. Joshi from the Delft University of Technology, NL for their valuable guidance on attaching reflective markers to the HSA.

References

[1] C. Della Santina, M. G. Catalano, *et al.*, "Soft robots," *Encyclopedia of Robotics*, vol. 489, 2020.

[2] S. Zaidi, M. Maselli, *et al.*, "Actuation technologies for soft robot grippers and manipulators: A review," *Current Robotics Reports*, vol. 2, no. 3, pp. 355–369, 2021.

[3] L. Chin, J. Lipton, *et al.*, "Compliant electric actuators based on handed shearing auxetics," in *2018 IEEE International Conference on Soft Robotics (RoboSoft)*. IEEE, 2018, pp. 100–107.

[4] R. L. Truby, L. Chin, and D. Rus, "A recipe for electrically-driven soft robots via 3d printed handed shearing auxetics," *IEEE Robotics and Automation Letters*, vol. 6, no. 2, pp. 795–802, 2021.

[5] A. Zhang, R. L. Truby, *et al.*, "Vision-based sensing for electrically-driven soft actuators," *IEEE Robotics and Automation Letters*, vol. 7, no. 4, pp. 11 509–11 516, 2022.

[6] I. Good, T. Brown-Moore, *et al.*, "Expanding the design space for electrically-driven soft robots through handed shearing auxetics," in *2022 International Conference on Robotics and Automation (ICRA)*. IEEE, 2022, pp. 10 951–10 957.

[7] D. T. Farrell, C. McGinn, and G. J. Bennett, "Extension twist deformation response of an auxetic cylindrical structure inspired by deformed cell ligaments," *Composite Structures*, vol. 238, p. 111901, 2020.

[8] F. Vanneste, O. Goury, and C. Duriez, "Enabling the control of a new degree of freedom by using anisotropic material on a 6-dof parallel soft robot," in *2021 IEEE 4th International Conference on Soft Robotics (RoboSoft)*. IEEE, 2021, pp. 636–642.

[9] C. Della Santina, C. Duriez, and D. Rus, "Model based control of soft robots: A survey of the state of the art and open challenges," *arXiv preprint arXiv:2110.01358*, 2021.

[10] M. Gazzola, L. Dudte, *et al.*, "Forward and inverse problems in the mechanics of soft filaments," *Royal Society open science*, vol. 5, no. 6, p. 171628, 2018. [Online]. Available: https://doi.org/10.1098/rsos.171628

[11] S. Grazioso, G. Di Gironimo, and B. Siciliano, "A geometrically exact model for soft continuum robots: The finite element deformation space formulation," *Soft robotics*, vol. 6, no. 6, pp. 790–811, 2019.

[12] S. H. Sadati, S. E. Naghibi, *et al.*, "Tmtdyn: A matlab package for modeling and control of hybrid rigid–continuum robots based on discretized lumped systems and reduced-order models," *The International Journal of Robotics Research*, vol. 40, no. 1, pp. 296–347, 2021.

[13] C. Armanini, C. Messer, *et al.*, "Soft robots modeling: a literature unwinding," *arXiv preprint arXiv:2112.03645*, 2021.

[14] F. Renda, F. Boyer, *et al.*, "Discrete cosserat approach for multisection soft manipulator dynamics," *IEEE Transactions on Robotics*, vol. 34, no. 6, pp. 1518–1533, 2018.

[15] R. J. Webster III and B. A. Jones, "Design and kinematic modeling of constant curvature continuum robots: A review," *The International Journal of Robotics Research*, vol. 29, no. 13, pp. 1661–1683, 2010.

[16] C. Della Santina and D. Rus, "Control oriented modeling of soft robots: The polynomial curvature case," *IEEE Robotics and Automation Letters*, vol. 5, no. 2, pp. 290–298, 2019.

[17] F. Renda, C. Armanini, *et al.*, "A geometric variable-strain approach for static modeling of soft manipulators with tendon and fluidic actuation," *IEEE Robotics and Automation Letters*, vol. 5, no. 3, pp. 4006–4013, 2020.

[18] A. Garg, I. Good, *et al.*, "Kinematic modeling of handed shearing auxetics via piecewise constant curvature," in *2022 IEEE 5th International Conference on Soft Robotics (RoboSoft)*. IEEE, 2022, pp. 423–430.

[19] N. Naughton, J. Sun, *et al.*, "Elastica: A compliant mechanics environment for soft robotic control," *IEEE Robotics and Automation Letters*, vol. 6, no. 2, pp. 3389–3396, 2021.

[20] A. T. Mathew, I. M. B. Hmida, *et al.*, "Sorosim: A matlab toolbox for hybrid rigid-soft robots based on the geometric variable-strain approach," *IEEE Robotics & Automation Magazine*, 2022.